

Theoretical Study of Bond-Switching in 1,6-Dihydro-6a-thia-1,6-diazapentalene (10-S-3) Systems Compared with Corresponding Oxygen Analogues

Teruo Atsumi,[1] Tomohiro Abe,[1] Kin-ya Akiba,[2] and Hiromi Nakai*[1,2]

[1]Department of Chemistry and Biochemistry, School of Advanced Science and Engineering, Waseda University, Tokyo 169-8555

[2]Research Institute for Science and Engineering, Waseda University, Tokyo 169-8555

Received January 7, 2010; E-mail: nakai@waseda.jp

Theoretical study of the mechanism of bond-switching of 5-(1-aminoethylimino)-3-methyl-1,2,4-thiadiazole and 5-(2-aminovinyl)isothiazole was carried out by using simplified models of 1,6-dihydro-6a-thia-1,6-diazapentalene (10-S-3) systems and corresponding oxygen analogs. Geometries and energetics were examined along unimolecular and bimolecular reaction paths by hybrid density functional theory (DFT) calculations with triple-zeta class basis sets by taking into account solvent effects which is estimated by the polarizable continuum model. It was clarified that the unimolecular reactions cannot proceed due to the high energy barriers around 70 kcal mol^{-1}. On the other hand, the bimolecular processes in neutral and acidic conditions can be accomplished for the sulfur compounds, not for the oxygen ones. The differences of the reactivities between the sulfur and oxygen compounds were found to be due to the difference of the stability of the symmetric intermediates with the hypervalent three-center four-electron bonds.

Bond-switching equilibration, i.e., ring transformation equilibrium, of a 5-(1-aminoethylimino)-3-methyl-1,2,4-thiadiazole (**1**) system, as shown in Scheme 1, was first reported[1,2] in 1979 and firmly established by the use of a $^{15}NH_2$ group.[3,4] Furthermore, it was found that the rate was extremely accelerated by acid. An intermediate **1**-B, which has 10-S-3 sulfurane (three coordinate hypervalent sulfurane bearing two equatorial lone pair electrons) consisting of a three-center four-electron (3c-4e) bond, was invoked to realize the equilibrium between **1**-A(α) and **1**-A(β).

The same type of bond-switching equilibration was reported for a 5-(2-aminovinyl)isothiazole (**2**) system,[5] as shown in Scheme 2, and detailed kinetic study was also carried out by using a $^{15}NH_2$ group.[6]

Since the discovery of bond-switching equilibration, a mechanism assuming consecutive 1,5-hydrogen shift (pathway A) has been proposed, based on the fact that the rate of equilibration is faster in a non-polar benzene solvent than in a polar dimethyl sulfoxide (DMSO) solvent. Pathway B was also shown to take part based on the shift of deuterium [N–D to C–D]. Such type of compounds **2**-B, i.e., Sulfurane-II, were synthesized as stable intermediates, in which two hydrogens are substituted by methyl groups (**3** and **4** in Chart 1).[7–10]

Attempts to estimate the hypervalent N–S–N bond energy was carried out by employing the skeleton of **1** fused with two pyrimidine rings (**5**), as shown in Scheme 3. The rotational barrier of this process was experimentally determined to be 16.6 kcal mol^{-1} (1 kcal mol^{-1} = 4.184 kJ mol^{-1}) by measuring coalescence of the two methyl groups.[11] The theoretical study[12] gave a close number, 15.7 kcal mol^{-1}. However, this process involves not only the bond change from the hypervalent N–S–N bond to the normal N–S single-bond but also the aromaticity change of the skeleton. Therefore, the hypervalent N–S–N bond energy itself could not been evaluated experimentally.

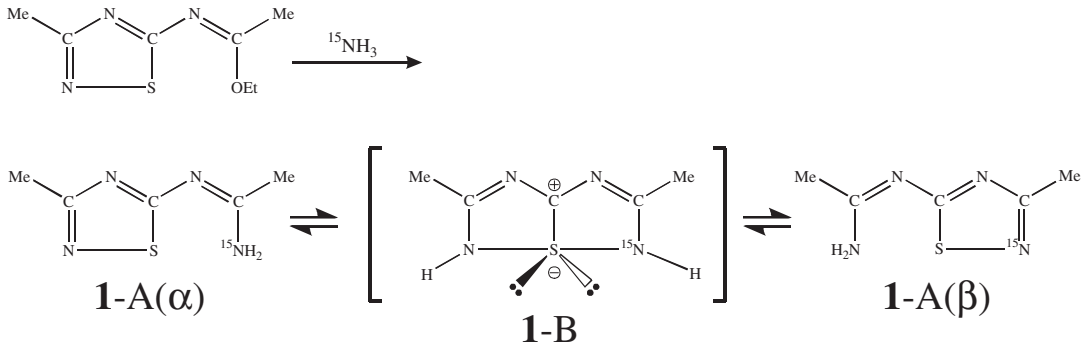

Scheme 1. Bond-switching equilibration of 5-(1-aminoethylimino)-3-methyl-1,2,4-thiadiazole (**1**) system.

Published on the web April 29, 2010; doi:10.1246/bcsj.20100006

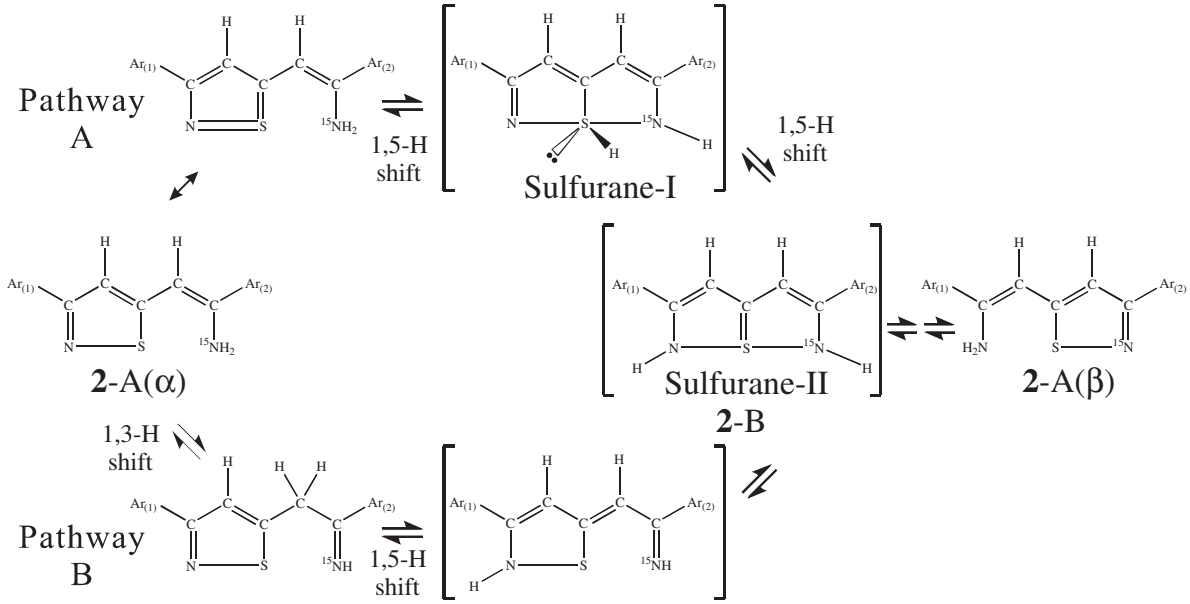

Scheme 2. Bond-switching equilibration of 5-(2-aminovinyl)isothiazole (**2**) system.

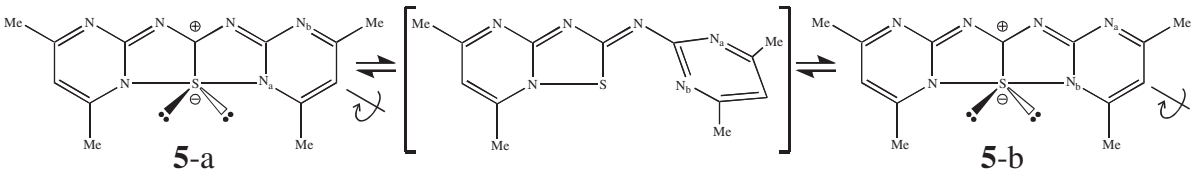

Scheme 3. Rotation of pyrimidine ring in **5**.

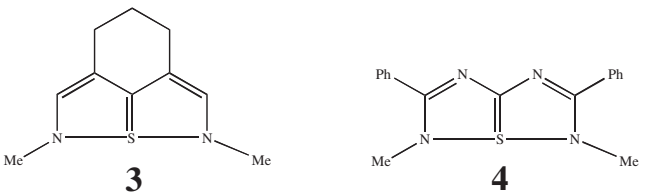

Chart 1. Structures of Sulfurane-II, **3** and **4**.

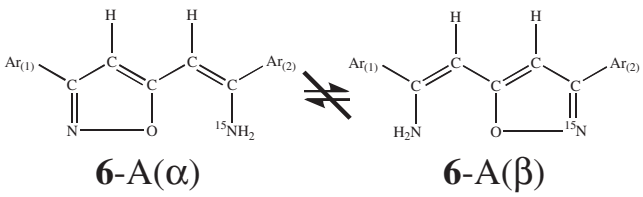

Scheme 4. Bond-switching equilibration of 1,2,4-oxadiazole and isoxazole (**6**) systems.

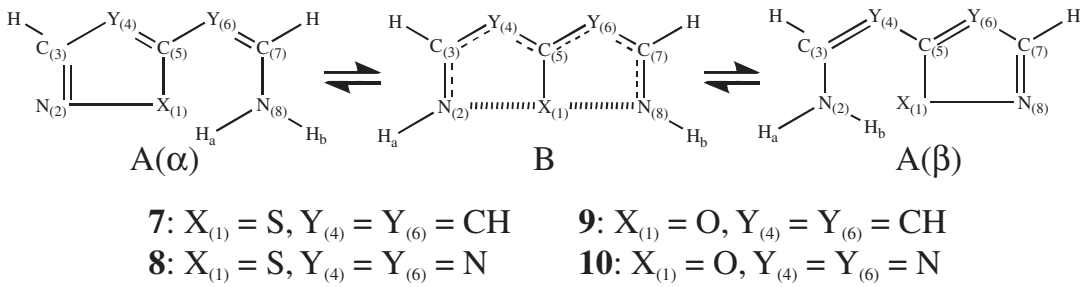

Scheme 5. Bond-switching equilibration of **7**–**10** systems.

On the other hand, such phenomenon cannot be found for the corresponding oxygen analogs, i.e., 1,2,4-oxadiazole and isoxazole systems (**6**) in Scheme 4.[6] The difference between **2** and **6** is only the center atom.

However, no experimental studies have been performed so far to detect or to scrutinize the 10-S-3 intermediate (Sulfurane-I or Sulfurane-II) in bond-switching equilibration between A(α) and A(β). The aim of this theoretical study is to clarify the reaction mechanism for the bond-switching equilibration on sulfur (**7** and **8**) and oxygen (**9** and **10**), employing simplified models as shown in Scheme 5.

In this model, the pathway from A(α) to B is the same as that from A(β) to B, because B is symmetric. We consider two types of pathways for each model. The first type is a unimolecular reaction path as described in Scheme 2. The second type is a bimolecular reaction path in neutral and acidic conditions.

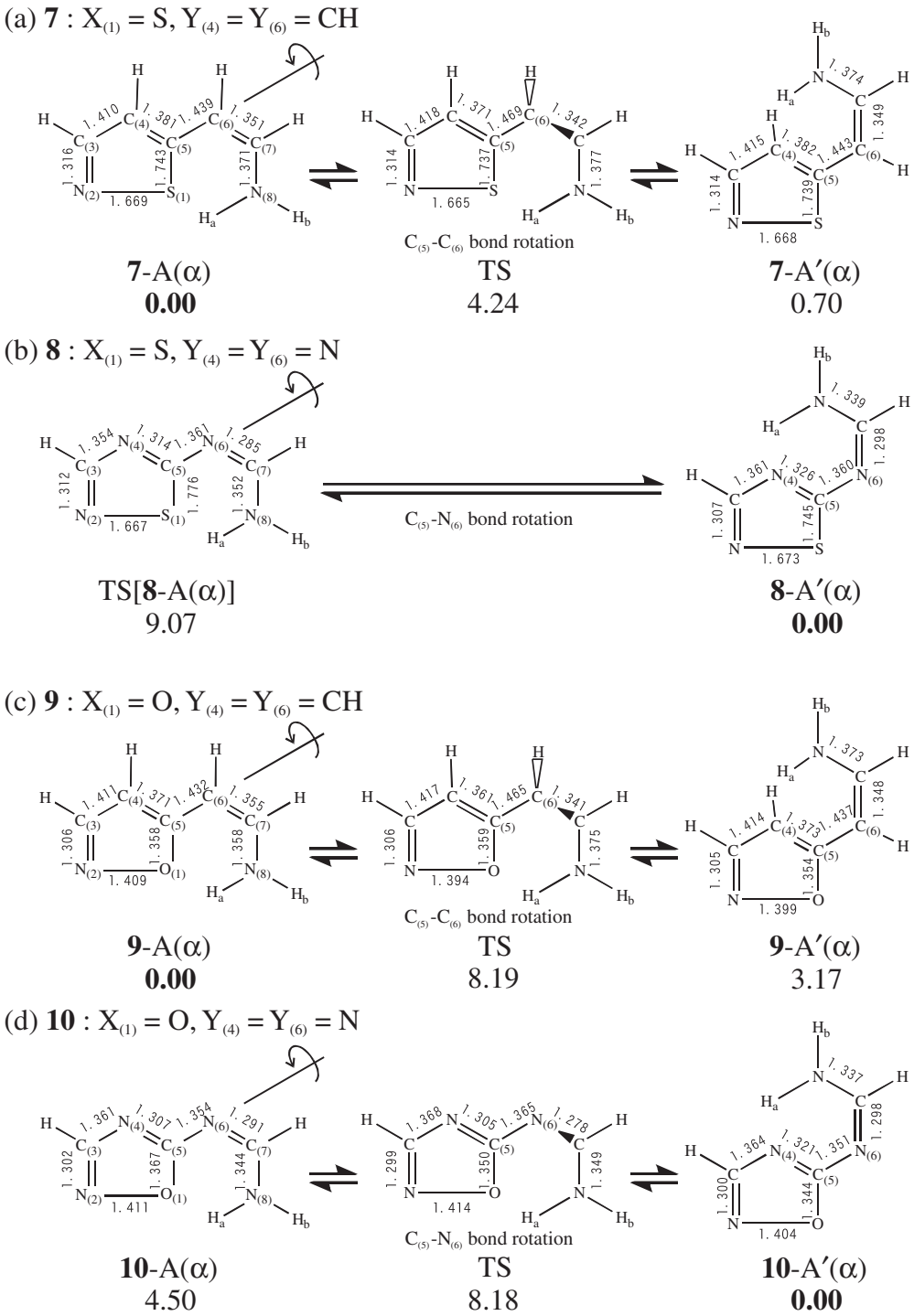

Figure 1. Geometries (in Å) and energetics (in kcal mol^{-1}) for the $C_{(5)}$–$Y_{(6)}$ rotation in **7**–**10**.

The organization of the present paper is as follows. The second section presents the computational methods adopted in this study. The third section describes the results and discussion, which involves the geometric structures of reactants, unimolecular reactions, bimolecular reactions in neutral and acidic conditions, and electronic structures and bond energies for the hypervalent intermediates. Concluding remarks are summarized in the last section.

Computational Details

This study theoretically examined both unimolecular and bimolecular reaction mechanisms for the bond-switching equilibrations of sulfur (**7** and **8**) and oxygen (**9** and **10**) compounds in Scheme 5, which involve two proton transfers from the right to the left nitrogen atoms. The bimolecular reactions were considered in neutral and acidic conditions for **7**.

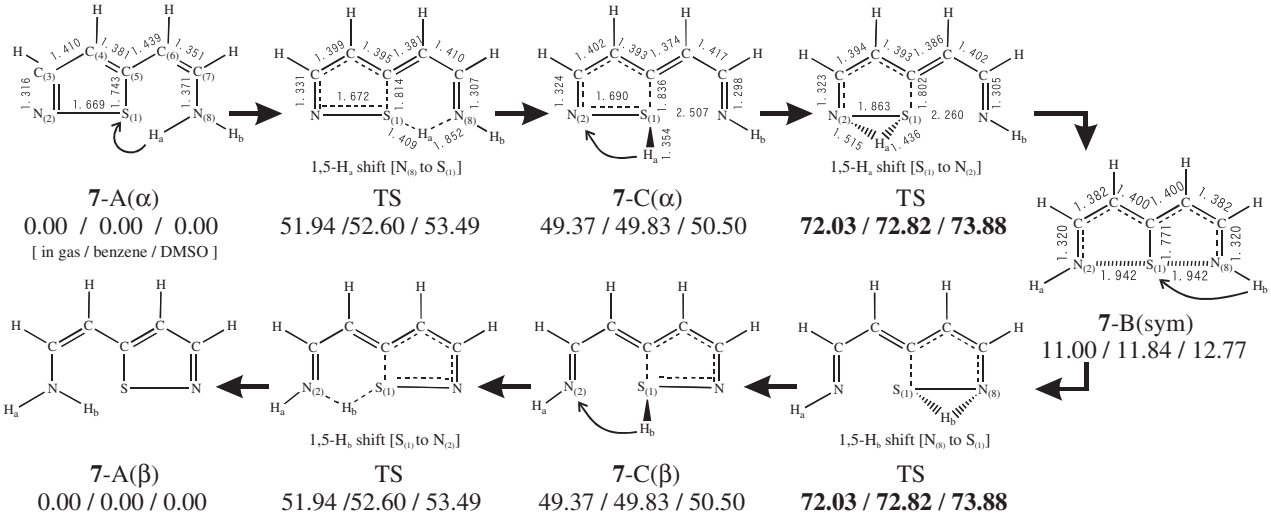

Figure 2. Geometries (in Å) and energetics (in kcal mol^{-1}) for the unimolecular bond-switching in **7**.

The geometries of expected intermediates as well as reactants and products were optimized by density functional theory (DFT) calculations with the B3LYP hybrid functional,[13] which consists of the Hartree–Fock exchange, the Slater exchange,[14] the Becke (B88) exchange,[15] the Vosko–Wilk–Nusair (VWN5) correlation,[16] and the Lee–Yang–Parr (LYP) correlation[17] functionals. The correlation consistent polarization plus valence triple zeta (cc-pVTZ) basis sets of Dunning[18,19] were adopted. In the geometry optimizations, solvent effects were not taken into account. Namely, the calculations correspond to a gas phase, or in other words, to an ideally non-polar solvent with the dielectric constant $\varepsilon = 1$.

The transition states (TSs) were also obtained at the same level of theory. Frequency analyses were performed to confirm the stable geometries without imaginary frequencies and the TSs with one imaginary one. Furthermore, to confirm that the obtained TSs connect with the adjacent intermediates, the intrinsic reaction coordinate (IRC) calculations were performed with the correlation consistent polarization plus valence double zeta (cc-pVDZ) basis sets.[20–24] The IRC results are presented in Supporting Information (Table 1S and Figures 1S–9S).

The solvent effects were calculated by using the integral equation formalism for the polarizable continuum model (PCM).[25–27] Single-point energy calculations fixing at the gas-phase geometries were performed with the solvent effects corresponding to benzene and DMSO: i.e., $\varepsilon = 2.247$ and 46.7 in the PCM, respectively. The above first-principle calculations were carried out in the Gaussian 03 suite of programs.[28]

Results and Discussion

Structure of Reactants. Starting compounds, **7**–**10**, are expected to have stable geometries of A(α) or A′(α). A′(α) forms are obtained by rotation of the $C_{(5)}$–$Y_{(6)}$ single-bond of A(α) forms. Figure 1 shows the optimized geometries of A(α), A′(α), and the TSs in between, which were obtained at the B3LYP/cc-pVTZ level of theory. Here, only the A′(α) form was obtained for **8**, while the others gave both structures. **8**-A(α) was obtained as a TS with the relative energy of 9.1 kcal mol^{-1}.

For **7** and **9** with $Y_{(4)} = Y_{(6)} = CH$, the A(α) form is more stable than A′(α), because of repulsion between hydrogen on $C_{(4)}$ and H_a on $N_{(8)}$ in the A′(α) form. On the other hand, A′(α) is more stable in **8** and **10** with $Y_{(4)} = Y_{(6)} = N$, in which the hydrogen-bonding interaction between $N_{(4)}$ and H_a is considered to stabilize the A′(α) form. The energy barriers with respect to the stable structures were estimated to be 4.2, 8.2, and 8.2 kcal mol^{-1} in **7**, **9**, and **10**, respectively. These small barriers suggest that the equilibrations between A(α) and A′(α) can be easily accomplished.

Unimolecular Reaction Path. We investigated a unimolecular reaction path from A(α)/A′(α) to A(β)/A′(β), which involves two hydrogen transfers. Geometries of intermediates for the stepwise hydrogen transfer and their corresponding TSs were obtained at the B3LYP/cc-pVTZ level of theory.

Figure 2 shows the obtained geometries for the reactant, product, intermediates, and corresponding TSs and their relative energies with respect to the reactant, **7**-A(α). The first intermediate **7**-C(α) bearing an $S_{(1)}$–H_a bond was obtained with relative energies of 49.4, 49.8, and 50.5 kcal mol^{-1} in the gas phase, benzene, and DMSO, respectively; hereafter, the energies in the three conditions are described as 49.4/49.8/50.5 kcal mol^{-1}. Relative energies of TS between **7**-A(α) and **7**-C(α) are 51.9/52.6/53.5 kcal mol^{-1}. As seen here, the solvent effect is comparatively small in this process: i.e., less than ca. 2 kcal mol^{-1}. The process is formally a 1,5-hydrogen shift which proceeds via pseudo six-member ring ($S_{(1)}$–$C_{(5)}$–$C_{(6)}$–$C_{(7)}$–$N_{(8)}$–H_a). **7**-C(α) corresponds to Sulfurane-I in Scheme 2, in which the $S_{(1)}$–H_a bond is out-of-plane and $S_{(1)}$–$N_{(2)}$ and $S_{(1)}$–$N_{(8)}$ distances are 1.690 and 2.507 Å, respectively. H_a further shifts to $N_{(2)}$ from $S_{(1)}$, yielding a symmetric intermediate **7**-B(sym) through the TS at 72.0/72.8/73.9 kcal mol^{-1}. This process is assigned to 1,5-hydrogen shift (or to 1,2-hydrogen shift). **7**-B(sym), which corresponds to Sulfurane II in Scheme 2, is relatively stable because of the hypervalent N–S–N bond as well as the π-electron delocalization.

A second hydrogen H_b transfers from $N_{(8)}$ to $S_{(1)}$ in the process between **7**-B(sym) and **7**-C(β). Due to the symmetry, the relative energies of the intermediates and TSs from

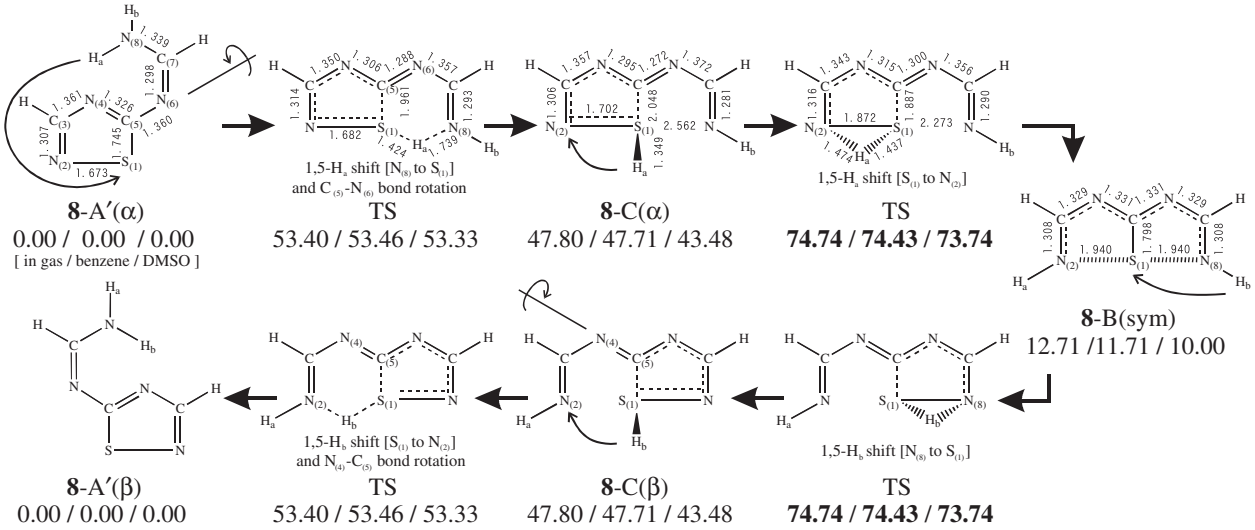

Figure 3. Geometries (in Å) and energetics (in kcal mol^{-1}) for the unimolecular bond-switching in **8**.

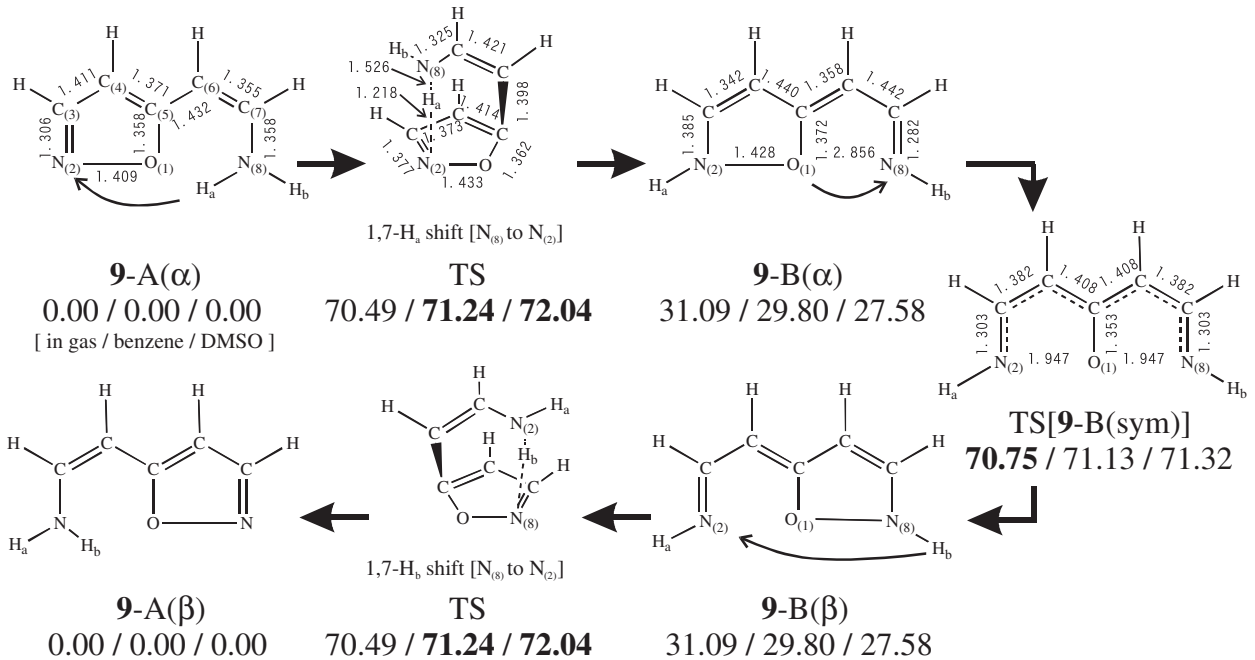

Figure 4. Geometries (in Å) and energetics (in kcal mol^{-1}) for the unimolecular bond-switching in **9**.

7-B(sym) to **7**-A(β) are equal to those of the corresponding states from **7**-A(α) to **7**-B(sym). The existence of the high barriers suggests that the unimolecular reactions from **7**-A(α) to **7**-A(β) are energetically unfavorable both with and without solvent effects.

Figure 3 describes the results for **8**. The pathway is similar to **7**, as shown in Figure 2. The main difference appears in the stable structure of the reactant as well as the product. The highest energy barriers of 74.7/74.4/73.7 kcal mol^{-1} suggest that the unimolecular processes are unfavorable both in the gas phase and in the benzene and DMSO solvents.

Figure 4 shows the results for **9**. The reactant and the product are described in the **9**-A(α) and **9**-A(β) forms, respectively. Contrary to the existence of the **7**-C(α) and **8**-C(α) intermediates with the S–H bond in Figures 2 and 3, such intermediates having the O–H bond could not be obtained in the process from **9**-A(α) to **9**-A(β). As a result, the hydrogen transfer occurs directly from $N_{(8)}$ to $N_{(2)}$ through a sterically congested TS, of which energies however are 70.5/71.2/72.0 kcal mol^{-1} higher than those of the reactants. The process is formally a 1,7-hydrogen shift. It should be notable that the intermediate **9**-B(α) with the $N_{(2)}$–H_a and $N_{(8)}$–H_b bonds possesses an asymmetric structure, in which the $N_{(2)}$–$O_{(1)}$ and $N_{(8)}$–$O_{(1)}$ distances are 1.428 and 2.856 Å, respectively, and the opposite is true for **9**-B(β). Furthermore, the symmetric structure of **9**-B(sym) is not a stable intermediate but a TS. It suggests that it is more difficult for oxygen to form hypervalent bonding than sulfur. The relative energies of 70.8/71.1/71.3 kcal mol^{-1} with respect to the reactant are comparable with those of the TS between **9**-A(α) and **9**-B(α). Because the

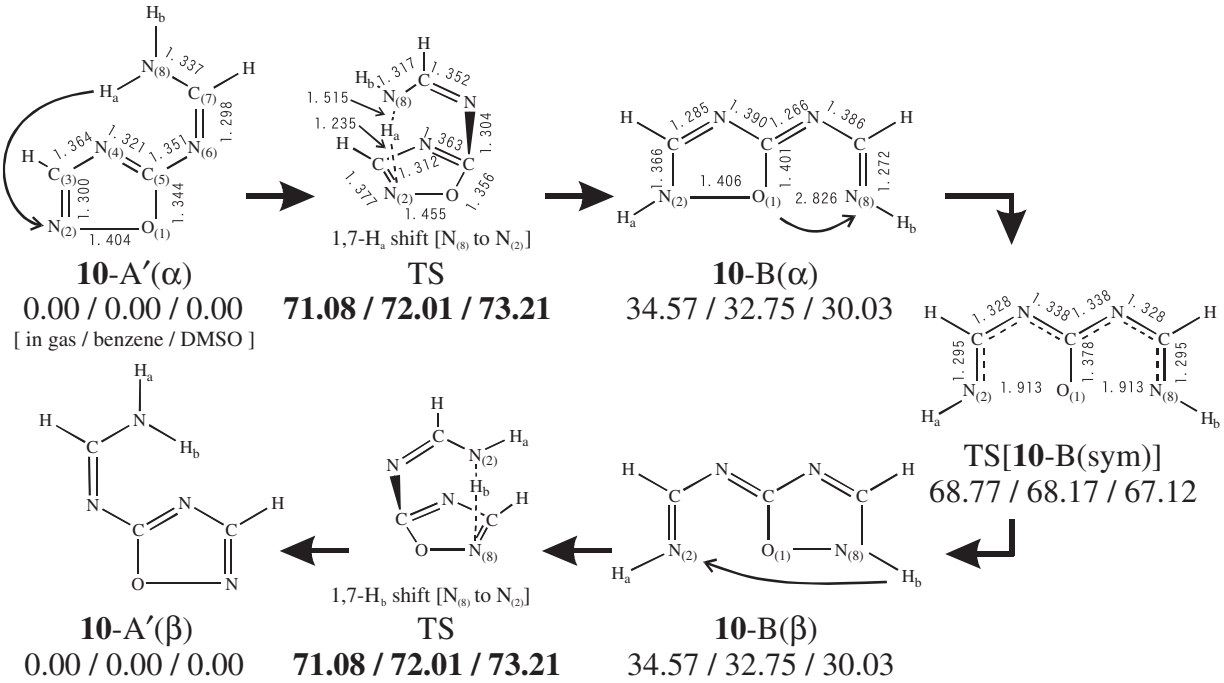

Figure 5. Geometries (in Å) and energetics (in kcal mol^{-1}) for the unimolecular bond-switching in **10**.

energy barrier estimated by the energy difference between the TS and the previous intermediate (or reactant) determines the kinetics in each primary step as the transition-state theory suggests, the first step shown in Figure 4 corresponds to a rate-determining process. The existence of high barriers in this process confirms the unreality of the unimolecular reaction.

Figure 5 describes the results for **10**. The reactant and the product are similar to **8**, as shown in Figure 3: i.e., A′(α) and A′(β) forms. The process in Figure 5 resembles that in Figure 4. Namely, the first hydrogen transfer, of which barriers are 71.1/72.0/73.2 kcal mol^{-1}, occurs directly from $N_{(8)}$ to $N_{(2)}$. The symmetric structure of **10**-B(sym) is a TS. The calculated data suggest the unreality of the process due to high barriers.

Figure 6 summarizes the energy diagrams for the unimolecular bond-switching reactions of **7**–**10**, as shown in Figures 2–5. In Figure 6a for **7** and Figure 6b for **8** with the center atom $X_{(1)} = S$, four 1,5-hydrogen shifts occur and **7**-B(sym) and **8**-B(sym) are obtained as stable intermediates. On the other hand, two 1,7-hydrogen shifts and one bond change are included in the pathway for **9** and **10** with $X_{(1)} = O$. In all cases, the highest barriers are around 70 kcal mol^{-1}. The solvent effect by benzene and DMSO leads minor change for the barriers. The substitutions at $Y_{(4)}$ and $Y_{(6)}$ do not change the energy diagrams in any significance except for the reactant and product structures. Therefore, it is concluded that the unimolecular bond-switching reactions cannot proceed thermally.

Bimolecular Reaction Path in Neutral Conditions. In this subsection, we investigated a bimolecular bond-switching reaction with two molecules of **7** in neutral conditions. Figure 7 shows geometries and relative energies in the bimolecular bond-switching reaction path of **7**. In the first step, two hydrogen bonds between H_c and $N_{(2)}$ and between H_a and $N_{(2)}$ are formed to create a dimer intermediate,

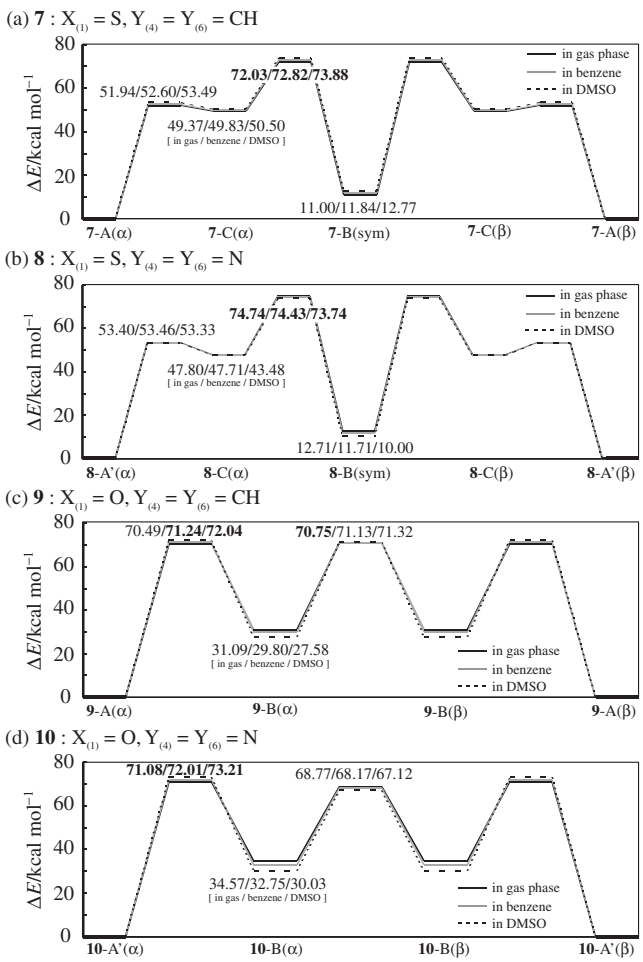

Figure 6. Energy diagrams (in kcal mol^{-1}) for the unimolecular bond-switching reactions in **7** (a), **8** (b), **9** (c), and **10** (d).

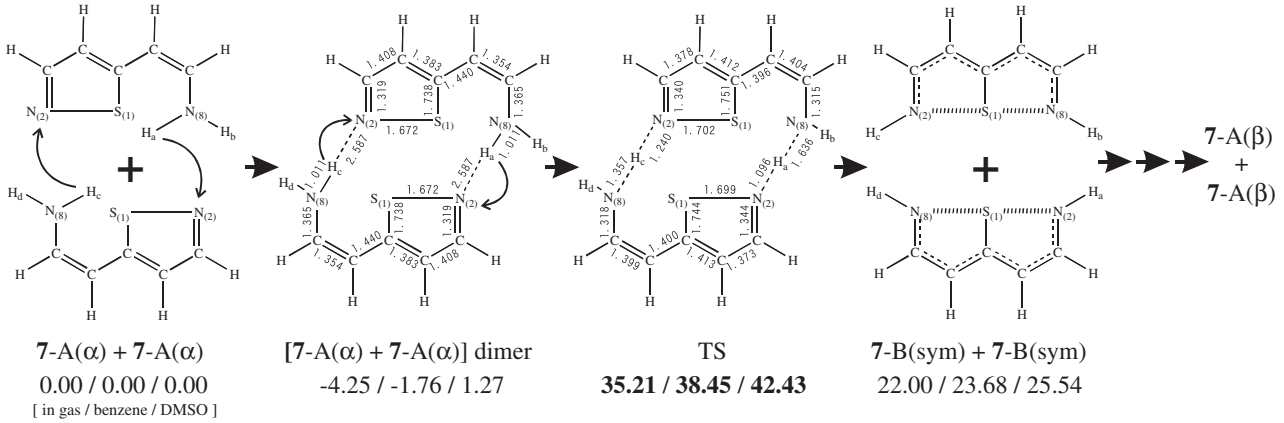

Figure 7. Geometries (in Å) and energetics (in kcal mol^{-1}) for the bimolecular bond-switching reaction of **7** in neutral conditions.

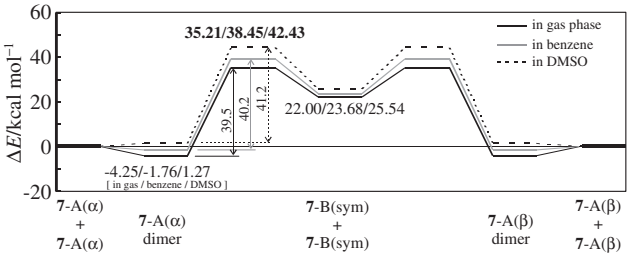

Figure 8. Energy diagrams (in kcal mol^{-1}) for the bimolecular bond-switching reaction of **7** in neutral conditions.

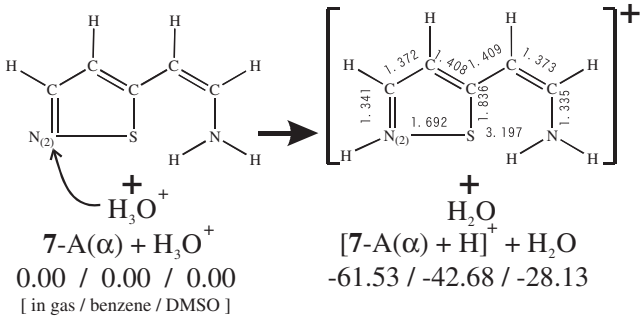

Figure 9. Geometries (in Å) and energetics (in kcal mol^{-1}) for the reaction of **7**-A(α) and H_3O^+.

[**7**-A(α) + **7**-A(α)], of which relative energies are $-4.3/-1.8/1.3$ kcal mol^{-1}. The stabilization energy by dimerizaiton is slightly larger in the non-polar solvent, benzene, than in the polar solvent, DMSO. In particular, the dimerizaiton in DMSO is an endothermic process. The geometry of [7-A(α) + 7-A(α)] dimer is symmetric. Next, both H_c and H_a shifts to $N_{(2)}$ in the upper and lower molecules, respectively, forming two **7**-B(sym). The relative energies of the TS and [**7**-B(sym) + **7**-B(sym)] intermediate are 35.2/38.5/42.4 and 22.0/23.7/25.5 kcal mol^{-1}, respectively. A symmetric structure could not be obtained for the TS. The asymmetric geometry of TS, in which $R(H_c–N_{(2)}) = 1.240$ Å and $R(H_a–N_{(2)}) = 1.096$ Å, indicates that hydrogen shifts of H_c and H_a take place concertedly, but with a timing gap. Two **7**-B(sym) change to two **7**-A(β) with the same reaction mechanism between two **7**-A(α) and two **7**-B(sym).

Figure 8 describes the energy diagram for the bimolecular bond-switching reaction of **7** in neutral conditions, as shown in Figure 7. The relative energies of intermediates and TSs in DMSO are higher than in benzene. The energy barriers are 39.5 [35.21 − (−4.25)], 40.2 [38.45 − (−1.76)], and 41.2 [42.43 − 1.27] kcal mol^{-1} in the gas phase, benzene, and DMSO, respectively. These barriers are remarkably smaller than those for the unimolecular reaction path, as discussed in the above section. Consequently, the present calculations suggest that the bimolecular reaction path can proceed thermally. Furthermore, the bimolecular bond-switching reaction in the benzene solvent is expected to be slightly faster than in the DMSO solvent, which is consistent with the experimental results.[6] By the same token, the bimolecular bond-switching reaction of **8** could occur. However, the bimolecular reactions of **9** and **10** cannot take place because of the existence of high barriers at **9**-B(sym) and **10**-B(sym).

Bimolecular Reaction Path in Acidic Conditions. In this subsection, we investigated a bimolecular reaction of **7** in acidic conditions, namely with a proton source H_3O^+. Although the previous experimental studies[6] used benzene and DMSO as solvents, a small amount of acid and/or water can be a contaminant even under carefully dried conditions. Thus, the model adopting H_3O^+ is thought to be reasonable in acidic conditions.

Figure 9 describes a product structure in a reaction between **7**-A(α) and H_3O^+. H^+ is transferred from H_3O^+ to $N_{(2)}$, generating [**7**-A(α) + H]$^+$ cation and H_2O. The heats of reaction are $-61.5/-42.7/-28.1$ kcal mol^{-1} in the gas phase, benzene, and DMSO, respectively. The exothermic behavior suggests that the [**7**-A(α) + H]$^+$ cation can be produced easily and quickly in acidic conditions. It should be noted that the process is considerably affected by the polarity of the solvent.

Next, we examined a bimolecular reaction with neutral **7**-A(α) and cationic [**7**-A(α) + H]$^+$, shown in Figure 10. The TSs could not be obtained in this case. H_a on $N_{(8)}$ in the [**7**-A(α) + H]$^+$ cation shifts to $N_{(2)}$ in the neutral **7**-A(α) through [**7**-A(α) + H + **7**-A(α)]$^+$ cation dimer, which has an asymmetric $N_{(8)}$–H_a–$N_{(2)}$ bond [1.028 and 1.914 Å]. The solvent effect is also of significance: namely, $-78.4/-51.9/-30.6$ kcal mol^{-1}. The decomposition of the cation dimer gives **7**-B(sym) and [**7**-A(α) + H]$^+$. By the same reaction mecha-

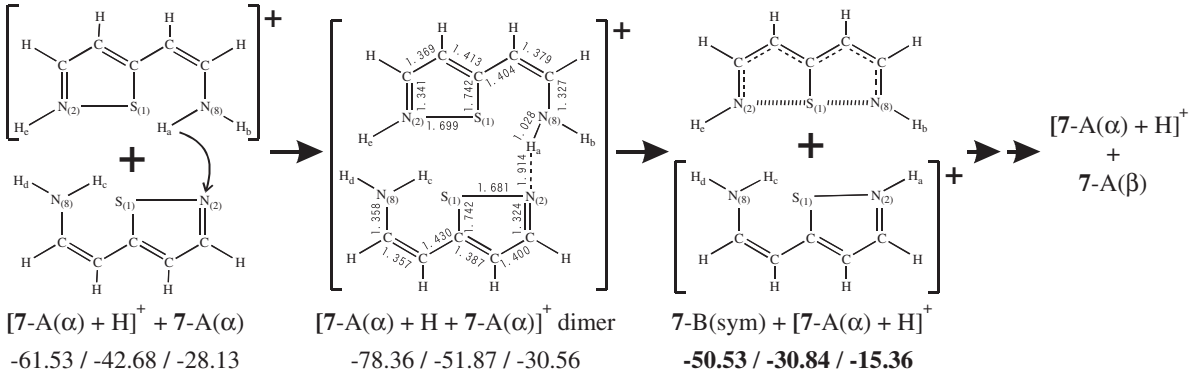

Figure 10. Geometries (in Å) and energetics (in kcal mol^{-1}) for the bimolecular bond-switching reaction of **7** in acidic conditions.

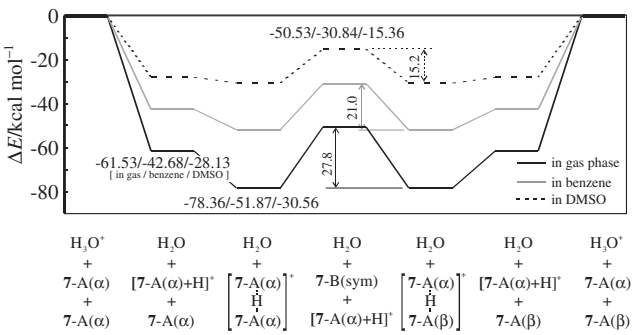

Figure 11. Energy diagrams (in kcal mol^{-1}) for the bimolecular bond-switching reaction of **7** in acidic conditions.

nism, **7**-A(β) and [**7**-A(α) + H]$^+$, of which relative energies are $-50.5/-30.8/-15.4$ kcal mol^{-1}, are produced.

Figure 11 summarizes the energy diagram for the bimolecular bond-switching reaction of **7** in acidic conditions, as shown in Figures 9 and 10. The three energy diagrams corresponding to the gas phase, benzene, and DMSO are apart from each other, in comparison with the neutral conditions in Figures 6 and 8. It indicates that the solvent effect is essential for the process. The first step, in which a proton transfers from H_3O^+ to **7**-A(α), is a considerably exothermic process. The second step giving the [**7**-A(α) + H + **7**-A(α)]$^+$ cation dimer is also exothermic. Although the third step is endothermic, the barrier heights are estimated to be 27.8 [$-50.53 - (-78.36)$], 21.0 [$-30.84 - (-51.87)$], and 15.2 [$-15.36 - (-30.56)$] kcal mol^{-1} in the gas phase, benzene, and DMSO, respectively. The barriers are significantly smaller than the bimolecular reaction in the neutral conditions shown in Figure 8: i.e., 39.5/40.2/41.2 kcal mol^{-1}. Therefore, it is concluded that the acid can greatly catalyze the bond-switching reaction, which agrees with the experimental study concerning **8**.[3,4] In a similar mechanism, the bimolecular bond-switching reaction of **8** is theoretically expected. On the contrary, it is speculated that the reaction of **9** and **10** cannot proceed easily because of the high barriers at **9**-B(sym) and **10**-B(sym). As a result, the stability of B(sym) plays a key role for the bond-switching reaction.

Molecular Orbitals for Hypervalent N–S–N Bond. The key compounds in the bond-switching equilibrations are B(sym) possessing the hypervalent 3c-4e bondings, in which four electrons enter bonding and non-bonding orbitals, and anti-bonding orbitals are unoccupied.[29–31] To confirm the 3c-4e interactions in **7**-B(sym) and **8**-B(sym), we examined the MOs corresponding to the bonding, non-bonding, and anti-bonding orbitals. Since the 3c-4e MOs further interact with other σ orbitals of two five-member rings, the three 3c-4e MOs are delocalized, as shown in Figure 12. The delocalization seems large in the bonding MOs: HOMO$-$6 in **7**-B(sym) and HOMO$-$7 in **8**-B(sym). It should be noted that the s orbital of S is mixing in the non-bonding MOs. The anti-bonding MOs, which are LUMO+2 in **7**-B(sym) and **8**-B(sym), are comparatively localized at the 3c-4e bond.

Bond Energy for Hypervalent N–S–N Bond. Finally, we estimated the strengths of hypervalent N–S–N bonds in **7**-B(sym) and **8**-B(sym). We examined two processes, namely, rotations of $C_{(5)}$–$Y_{(6)}$ double-bond and $Y_{(6)}$–$C_{(7)}$ single-bond. In addition to the double-/single-bond rotation, these processes involve the cleavage of $S_{(1)}$–$N_{(8)}$ bond, and the changing of $S_{(1)}$–$N_{(2)}$ bond from a hypervalent-type interaction to a normal single-bond. Figure 13 shows the geometries of the compounds in these reactions and their relative energies with respect to **7**-A(α)/**8**-A(α) at the B3LYP/cc-pVTZ level of theory. These calculations do not include a solvent effect, which is expected not to be of importance for these neutral compounds. The relative energies of the TSs are also described in the figure.

In both cases, the barriers for the double-bond rotations are higher than those for the single-bond rotations as expected. It should be noted that the energies of the products, namely, B′ and B″, are sufficiently close to each other: namely, (22.5, 22.5) for (**7**-B′, **7**-B″) and (30.4, 28.8) for (**8**-B′, **8**-B″) in kcal mol^{-1}, respectively. This indicates that the skeleton differences between B′ and B″ demonstrated sufficiently small changes in energy. As a result, the energy difference between B(sym) and B′/B″ mainly comes from the hypervalent N–S–N bond and the N–S single-bond. Since the N–S single-bond energy was observed to be 33.2 kcal mol^{-1} in HSNO,[32] the hypervalent N–S–N bond energy is approximately estimated to be 44.7 and 50.1 kcal mol^{-1} in **7**-B(sym) and **8**-B(sym), respectively.[33]

Conclusion

The bond-switching equilibrations between A(α) and A(β) of 5-(1-aminoethylimino)-3-methyl-1,2,4-thiadiazole (**1**) and 5-(2-aminovinyl)isothiazole (**2**) systems were investigated

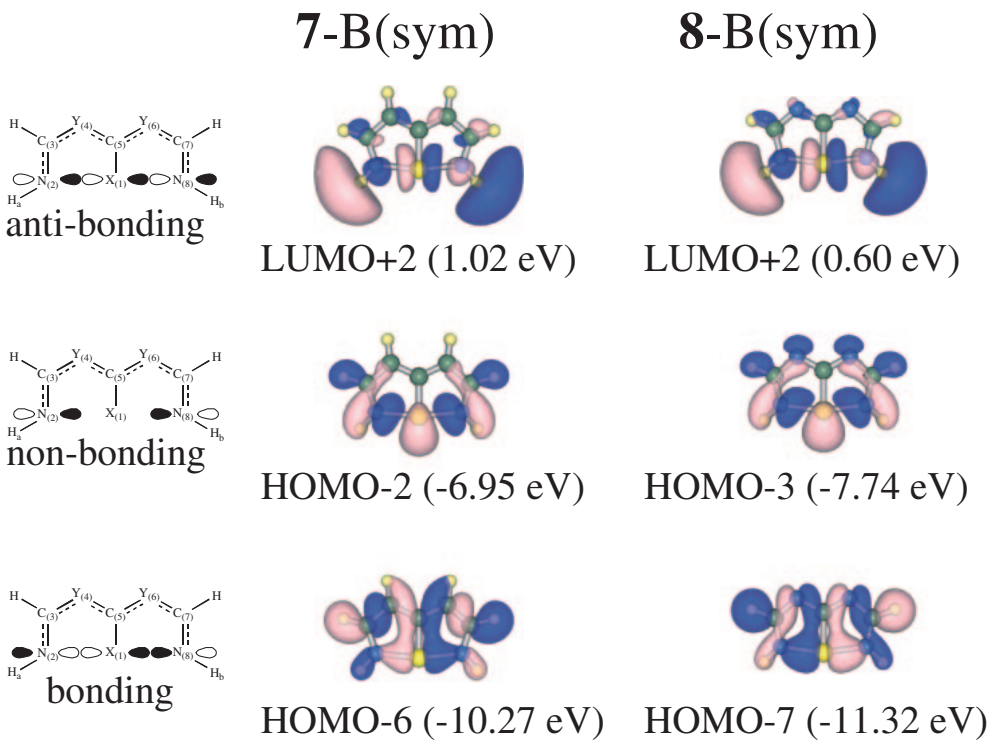

Figure 12. Bonding, non-bonding, and anti-bonding orbitals for the hypervalent N–S–N bond.

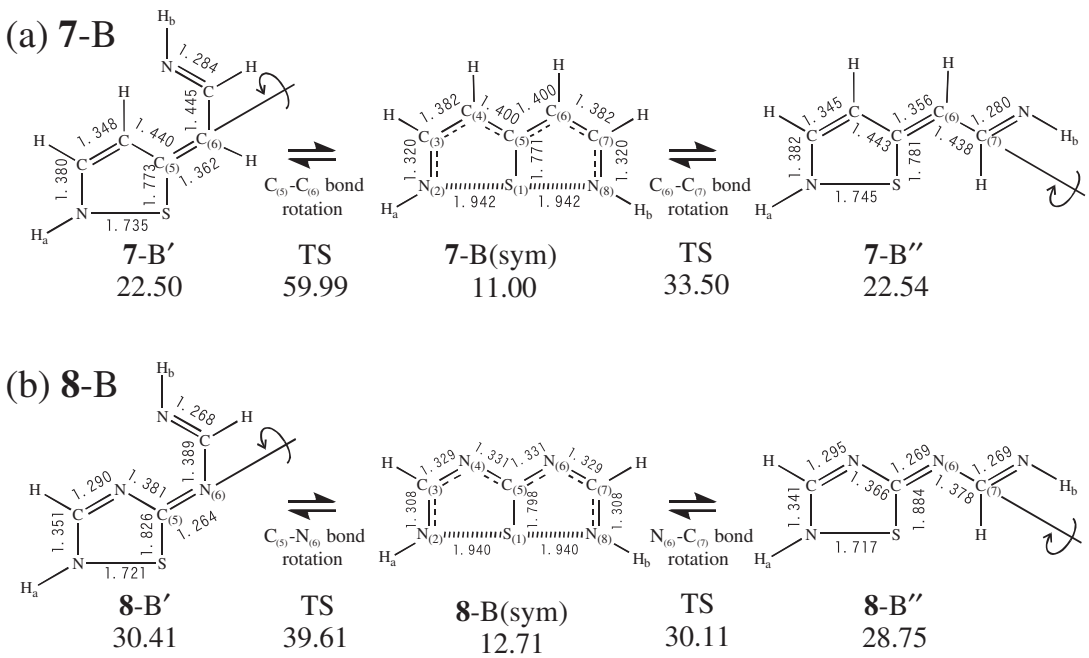

Figure 13. Geometries (in Å) and energetics (in kcal mol^{-1}) for the $C_{(5)}$–$Y_{(6)}$ and $Y_{(6)}$–$C_{(7)}$ rotations in **7**-B(sym) and **8**-B(sym).

theoretically using model compounds of **7** ($X_{(1)}$ = S, $Y_{(4)}$ = $Y_{(6)}$ = CH), **8** ($X_{(1)}$ = S, $Y_{(4)}$ = $Y_{(6)}$ = N), **9** ($X_{(1)}$ = O, $Y_{(4)}$ = $Y_{(6)}$ = CH), and **10** ($X_{(1)}$ = O, $Y_{(4)}$ = $Y_{(6)}$ = N) in Scheme 5. Due to the hydrogen bonding, the stable geometries of the reactants in **8** and **10** are different from those in **7** and **9**. The present results confirm that the unimolecular reactions cannot proceed due to the high energy barriers with/without solvent effects. On the contrary, the bimolecular processes with two molecules of **7** as well as **8** can be accomplished in neutral and acidic conditions, while they cannot in **9** and **10** with the O center. These differences originate from the stability of the hypervalent N–S–N bond. The existences of the hypervalent 3c-4e N–S–N bonds were confirmed by the MO analysis. Furthermore, the strengths of the N–S–N bonds were evaluated.

Some of the present calculations were performed at the Research Center for Computational Science (RCCS), Okazaki Research Facilities, and National Institutes of Natural Sciences (NINS). This study was supported in part by a Grant-in-Aid for Scientific Research on Priority Areas "Molecular Theory for Real Systems" KAKENHI 18066016 from the Ministry of Education, Culture, Sports, Science and Technology (MEXT), Japan; by the Nanoscience Program in the Next Generation Super Computing Project of the MEXT; by the Global Center Of Excellence (GCOE) "Practical Chemical Wisdom" from the MEXT; by a Waseda University Grant for Special Research Projects (Project number: 2009B-102); and by a project research grant for the "Development of high-performance computational environment for quantum chemical calculation and its assessment" from the Research Institute for Science and Engineering (RISE), Waseda University.

Supporting Information

Imaginary frequencies of TSs by frequency analysis and IRC trajectories. This material is available free of charge on the Web at: http://www.csj.jp/journals/bcsj/.

References

1 K.-y. Akiba, T. Kobayashi, S. Arai, *J. Am. Chem. Soc.* **1979**, *101*, 5857.
2 F. Iwasaki, K.-y. Akiba, *Acta Crystallogr., Sect. B* **1981**, *37*, 185.
3 Y. Yamamoto, K.-y. Akiba, *J. Am. Chem. Soc.* **1984**, *106*, 2713.
4 Y. Yamamoto, K.-y. Akiba, *Bull. Chem. Soc. Jpn.* **1989**, *62*, 479.
5 K. Ohkata, Y. Ohyama, Y. Watanabe, K.-y. Akiba, *Tetrahedron Lett.* **1984**, *25*, 4561.
6 K.-y. Akiba, K. Kashiwagi, Y. Ohyama, Y. Yamamoto, K. Ohkata, *J. Am. Chem. Soc.* **1985**, *107*, 2721.
7 F. Iwasaki, K.-y. Akiba, *Bull. Chem. Soc. Jpn.* **1984**, *57*, 2581.
8 A. Hordvik, K. Julshamn, *Acta Chem. Scand.* **1972**, *26*, 343.
9 K.-y. Akiba, Y. Yamamoto, *Heteroat. Chem.* **2007**, *18*, 161.
10 *Chemistry of Hypervalent Compounds*, ed. by K.-y. Akiba, Wiley-VCH, New York, **1999**.
11 K. Ohkata, M. Ohsugi, K. Yamamoto, M. Ohsawa, K.-y. Akiba, *J. Am. Chem. Soc.* **1996**, *118*, 6355.
12 Y. Yamauchi, K.-y. Akiba, H. Nakai, *Chem. Lett.* **2007**, *36*, 1120.
13 A. D. Becke, *J. Chem. Phys.* **1993**, *98*, 5648.
14 J. C. Slater, *Phys. Rev.* **1951**, *81*, 385.
15 A. D. Becke, *Phys. Rev. A* **1988**, *38*, 3098.
16 S. H. Vosko, L. Wilk, M. Nusair, *Can. J. Phys.* **1980**, *58*, 1200.
17 C. Lee, W. Yang, R. G. Parr, *Phys. Rev. B* **1988**, *37*, 785.
18 T. H. Dunning, Jr., *J. Chem. Phys.* **1989**, *90*, 1007.
19 D. E. Woon, T. H. Dunning, Jr., *J. Chem. Phys.* **1993**, *98*, 1358.
20 K. Fukui, *J. Phys. Chem.* **1970**, *74*, 4161.
21 K. Fukui, S. Kato, H. Fujimoto, *J. Am. Chem. Soc.* **1975**, *97*, 1.
22 S. Kato, K. Morokuma, *J. Chem. Phys.* **1980**, *73*, 3900.
23 C. Gonzalez, H. B. Schlegel, *J. Chem. Phys.* **1989**, *90*, 2154.
24 C. Gonzalez, H. B. Schlegel, *J. Phys. Chem.* **1990**, *94*, 5523.
25 M. T. Cancès, B. Mennucci, J. Tomasi, *J. Chem. Phys.* **1997**, *107*, 3032.
26 M. Cossi, V. Barone, B. Mennucci, J. Tomasi, *Chem. Phys. Lett.* **1998**, *286*, 253.
27 B. Mennucci, J. Tomasi, *J. Chem. Phys.* **1997**, *106*, 5151.
28 M. J. Frisch, G. W. Trucks, H. B. Schlegel, G. E. Scuseria, M. A. Robb, J. R. Cheeseman, J. A. Montgomery, Jr., T. Vreven, K. N. Kudin, J. C. Burant, J. M. Millam, S. S. Iyengar, J. Tomasi, V. Barone, B. Mennucci, M. Cossi, G. Scalmani, N. Rega, G. A. Petersson, H. Nakatsuji, M. Hada, M. Ehara, K. Toyota, R. Fukuda, J. Hasegawa, M. Ishida, T. Nakajima, Y. Honda, O. Kitao, H. Nakai, M. Klene, X. Li, J. E. Knox, H. P. Hratchian, J. B. Cross, V. Bakken, C. Adamo, J. Jaramillo, R. Gomperts, R. E. Stratmann, O. Yazyev, A. J. Austin, R. Cammi, C. Pomelli, J. W. Ochterski, P. Y. Ayala, K. Morokuma, G. A. Voth, P. Salvador, J. J. Dannenberg, V. G. Zakrzewski, S. Dapprich, A. D. Daniels, M. C. Strain, O. Farkas, D. K. Malick, A. D. Rabuck, K. Raghavachari, J. B. Foresman, J. V. Ortiz, Q. Cui, A. G. Baboul, S. Clifford, J. Cioslowski, B. B. Stefanov, G. Liu, A. Liashenko, P. Piskorz, I. Komaromi, R. L. Martin, D. J. Fox, T. Keith, M. A. Al-Laham, C. Y. Peng, A. Nanayakkara, M. Challacombe, P. M. W. Gill, B. Johnson, W. Chen, M. W. Wong, C. Gonzalez, J. A. Pople, *Gaussian 03, Revision C.02*, Gaussian, Inc., Wallingford CT, **2004**.
29 G. C. Pimentel, *J. Chem. Phys.* **1951**, *19*, 446.
30 R. J. Hach, R. E. Rundle, *J. Am. Chem. Soc.* **1951**, *73*, 4321.
31 F. Weinhold, C. R. Landis, *Valency and Bonding*, Cambridge Univ. Press, New York, **2005**, Chap. 3.5.
32 *Handbook of Chemistry and Physics*, 88th ed., ed. by D. R. Lide, CRC, London, **2008**, pp. 9–67.
33 The values are estimated as follows. For example, in **7**-B(sym); E(N–S–N) − E(N–S) = (22.54 + 22.50)/2 − 11.00 = 11.5 (Calc.), and E(HS–NO) = 33.2 kcal mol^{-1} (Exptl.), then, E(N–S–N) = 44.7 kcal mol^{-1}. Similarly, in **8**-B(sym), E(N–S–N) = 16.9 + 33.2 = 50.1 kcal mol^{-1}.